



Lactate promotes invasive *Klebsiella pneumoniae* liver abscess syndrome by increasing capsular polysaccharide biosynthesis via the PTS-CRP axis

Received: 1 November 2024

Accepted: 19 June 2025

Published online: 01 July 2025

 Check for updatesJunying Zhu^{1,2,5}, Guangyu Wang^{3,5}, Wei Xi¹, Zhen Shen¹, Qing Wei¹,
Xiaoqiong Fang⁴ & Min Li^{1,2,4}  

The global incidence of invasive *Klebsiella pneumoniae* liver abscess syndrome (IKPLAS) increases, yet its underlying molecular mechanisms remain elusive, hindering the development of effective therapeutic strategies. In this study, we analyze bacterial molecular profiles and clinical data from patients with KPLA and IKPLAS, and find no significant difference in the molecular characteristics of *K. pneumoniae* between the two groups, however, we identify elevated blood lactate levels as an independent predictor of IKPLAS. Further investigation reveals that lactate enhances *K. pneumoniae* virulence by promoting capsular polysaccharide (CPS) biosynthesis. Mechanistically, lactate reduces cyclic adenosine monophosphate (cAMP) levels by downregulating the expression of mannose-specific phosphotransferase system (man-PTS) enzyme IIA-D genes (*gfrA*, *gfrB*, *gfrC* and *gfrD*). This reduction in cAMP levels enhances CPS biosynthesis by decreasing its binding to the cAMP receptor protein (CRP). Our results highlight lactate's role in enhancing the virulence of *K. pneumoniae* via the PTS-CRP axis, offering insights into the pathogenesis of IKPLAS.

The rise of liver abscess (LA) poses an urgent public health challenge worldwide, particularly in Asia, where incidence rates are climbing rapidly^{1–4}. Over the past three decades, *Klebsiella pneumoniae* has emerged as the leading cause of LA, with ~20% of cases progressing to extrahepatic migratory infections (EMIs), such as endophthalmitis, meningitis and necrotizing fasciitis, collectively known as invasive *K. pneumoniae* liver abscess syndrome (IKPLAS)^{5–7}. Despite aggressive treatment regimens, mortality rates for IKPLAS remain as high as 20%, and many survivors suffer from debilitating complications, including central nervous system damage and permanent blindness^{8–12}.

The hypervirulence of *K. pneumoniae* plays a critical role in the progression of IKPLAS, highlighting the need to understand the factors regulating virulence in these strains. Capsular polysaccharide (CPS) and siderophores are well-known virulence factors in *K. pneumoniae*, essential for its pathogenicity¹³. The CPS gene cluster comprises ~17 or more open reading frames (ORFs), organized into three operons, each regulated by a promoter located upstream of *orf1* (*galF*), *orf3* (*wzi*), and *orf16* (*manC*)¹⁴. Aerobactin, along with other siderophores such as enterobactin, yersiniabactin and salmochelin, further contributes to the hypervirulence of *K. pneumoniae*, enhancing its ability to cause severe infections^{15,16}. As these virulence factors are directly involved in

¹Department of Laboratory Medicine, Ren Ji Hospital, School of Medicine, Shanghai Jiao Tong University, Shanghai, China. ²Faculty of Medical Laboratory Science, College of Health Science and Technology, School of Medicine, Shanghai Jiao Tong University, Shanghai, China. ³Department of Cardiology, Renji Hospital, School of Medicine, Shanghai Jiao Tong University, Shanghai, China. ⁴School of Nursing, Shanghai Jiao Tong University, Shanghai, China. ⁵These authors contributed equally: Junying Zhu, Guangyu Wang. ✉e-mail: rjlimin@shsmu.edu.cn

disease progression, understanding their regulation is critical for developing novel interventions to combat IKPLAS and reduce associated morbidity and mortality.

Previous research on IKPLAS has predominantly focused on clinical presentations, treatments and microbial characteristics of *K. pneumoniae*, often limited to case reports^{17–20}. While C-P Fung et al. identified *K. pneumoniae* serotype K1, the hypermucoviscous phenotype (HMV) and CPS as significantly associated with IKPLAS, these microbial features alone cannot fully account for the pathogenesis, as non-K1 *K. pneumoniae* strains have also been implicated in the syndrome^{21,22}. More recently, the type VI secretion system (T6SS) in *K. pneumoniae* has been suggested to contribute to IKPLAS development through interactions with host factors²³. High morbidity and mortality of IKPLAS necessitates a study of exploring the dynamic interactions between microbial and host factors, which likely contribute to IKPLAS.

Our study directly addresses this knowledge gap by systematically investigating both microbial and host factors involved in IKPLAS. We observed that elevated lactate level, a well-established biomarker for sepsis severity, as an independent risk factor for IKPLAS. Further investigation revealed that lactate enhanced the virulence of *K. pneumoniae* through the phosphoenolpyruvate phosphotransferase system (PTS)-cyclic Adenosine monophosphate (cAMP) response protein (CRP)-CPS axis, potentially explaining the progression of IKPLAS. Our findings offer insights into the pathogenesis of IKPLAS and highlight a potential target for therapeutic intervention in this life-threatening infection.

Results

Clinical data of patients with KPLA and bacterial collection

Among the 68 patients diagnosed with LA caused by *K. pneumoniae*, 30 patients with EMIs, including 22 with sepsis and 8 with both sepsis and pulmonary infection, were assigned to the IKPLAS group. The remaining 38 patients were included in the KPLA group. Clinical data analysis revealed that patients in the IKPLAS group were older, had a higher prevalence of diabetes mellitus, elevated levels of blood glycated hemoglobin (HbA1c) and blood lactate, less frequent administration of moxifloxacin during treatment, and underwent a greater number of puncture procedures compared to those in the KPLA group (Supplementary Table 1). A total of 68 non-repetitive *K. pneumoniae* isolates were collected from the blood or pus of the patients, including 30 isolates from the IKPLAS group and 38 isolates from the KPLA group, for subsequent analysis.

No significant differences in the molecular characteristics and antibiotic susceptibility of *K. pneumoniae* isolated from patients in IKPLAS and KPLA groups

HMV phenotype was observed in 83.3% (25/30) *K. pneumoniae* isolates from the IKPLAS group and 78.9% (30/38) isolates from the KPLA group ($P > 0.05$) (Fig. 1a, b). Sequence type (ST) 23 and K1 were the predominant clone and serotype in both groups, with no statistically significant difference in their proportions ($P > 0.05$) (Fig. 1c, d). No significant differences were found in the carriage of virulence or resistance genes between the isolates from the two groups ($P > 0.05$). The above statistical results are detailed in Supplementary Table 2. Additionally, more than half of the isolates in both groups exhibited a virulence score of 5 and a resistance score of 0. However, the proportion of isolates with these scores did not differ significantly between the two groups ($P > 0.05$), as determined by Kleborate²⁴ (Fig. 1e, f). Except for one isolate that exhibited resistance to carbapenems, all other 67 isolates were highly sensitive to commonly used antibiotics (Supplementary Table 3). These findings indicated that bacterial characteristics alone were not the primary drivers of IKPLAS, suggesting that alternative factors, potentially host-related, could play a pivotal role.

Phylogenetic relatedness

To investigate the clonal relatedness of our isolates in the context of the published populations, we downloaded 49 genome sequences of *K. pneumoniae* isolates associated with LA from the Sequence Read Archive (SRA) database. These isolates originated from Singapore ($n = 43$), Czechia ($n = 3$), Ireland ($n = 2$) and Portugal ($n = 1$). Detailed metadata on all 117 isolates, including our 68 isolates and the 49 global isolates is provided in Supplementary data files. A single nucleotide polymorphism (SNP) tree was constructed using all the 117 genomes. As shown in Fig. 2, distinct phylogenetic clusters were observed for each ST, including ST23, ST65 and ST86. Notably, each cluster, especially the largest ST23 cluster, contained isolates from our study as well as from several other countries, suggesting similar distribution patterns across various countries. Furthermore, our isolates were genetically closely related to those from other countries, indicating that the *K. pneumoniae* isolates in our study are representative of the global strains.

Elevated blood lactate levels as an independent risk factor for IKPLAS

To identify host factors associated with IKPLAS, we conducted univariate and multivariate analyses of potential risk factors. Our findings revealed that elevated blood lactate levels, reduced moxifloxacin administration and a greater number of puncture procedures were independently associated with IKPLAS (Table 1). Among these factors, blood lactate levels warrant particular attention due to their emerging role in enhancing the virulence of various pathogens^{25–27}. To further establish the association between lactate and IKPLAS, we compared blood lactate levels in patients with IKPLAS to those in the general population, and found significantly higher lactate levels in the IKPLAS group. Moreover, blood lactate levels in patients with IKPLAS were markedly higher than in patients with respiratory tract infections (RTIs) or urinary tract infections (UTIs) caused by *K. pneumoniae* (Supplementary Fig. 1). Hyperlactatemia reflects elevated lactate levels in the liver abscess microenvironment. Therefore, we propose that lactate, a previously underexplored factor, may play a critical role in driving IKPLAS within the liver abscess microenvironment.

Lactate promotes CPS biosynthesis and enhances the anti-phagocytic properties of *K. pneumoniae*

Building on previous evidence that lactate enhances microbial pathogenicity by upregulating key virulence factors²⁸, we hypothesized that lactate contributes to the development of IKPLAS by modulating virulence genes expression. To identify specific virulence factors regulated by lactate, CPS production and gene expression were assessed in 10 randomly selected *K. pneumoniae* clinical isolates cultured in Luria-Bertani (LB) broth with increasing concentrations of sodium lactate. The detailed information about the isolates is in Supplementary Table 4. Sodium lactate was used to control for pH effects. All isolates showed peak CPS production at 40 mM sodium lactate (Fig. 3a). The HMV phenotype was also enhanced under these conditions compared to LB alone (Fig. 3b). CPS gene cluster expression increased 1.5- to 3-fold in 40 mM sodium lactate compared to LB alone (Fig. 3c–e). In contrast, siderophore-related gene expression remained unchanged (Supplementary Fig. 2) and growth assays under iron-restricted conditions revealed no significant difference between the groups (Supplementary Fig. 3). These findings suggest that lactate enhances *K. pneumoniae* virulence primarily by promoting CPS production rather than siderophore regulation. For subsequent experiments, we used LB supplemented with 40 mM sodium lactate (referred to as Lac-LB) to investigate the regulatory mechanisms of lactate on CPS production.

CPS protects the bacteria from phagocytosis and killing by host factors²⁹. To explore the effect of lactate on the anti-phagocytic properties of *K. pneumoniae*, we performed phagocytosis assay and

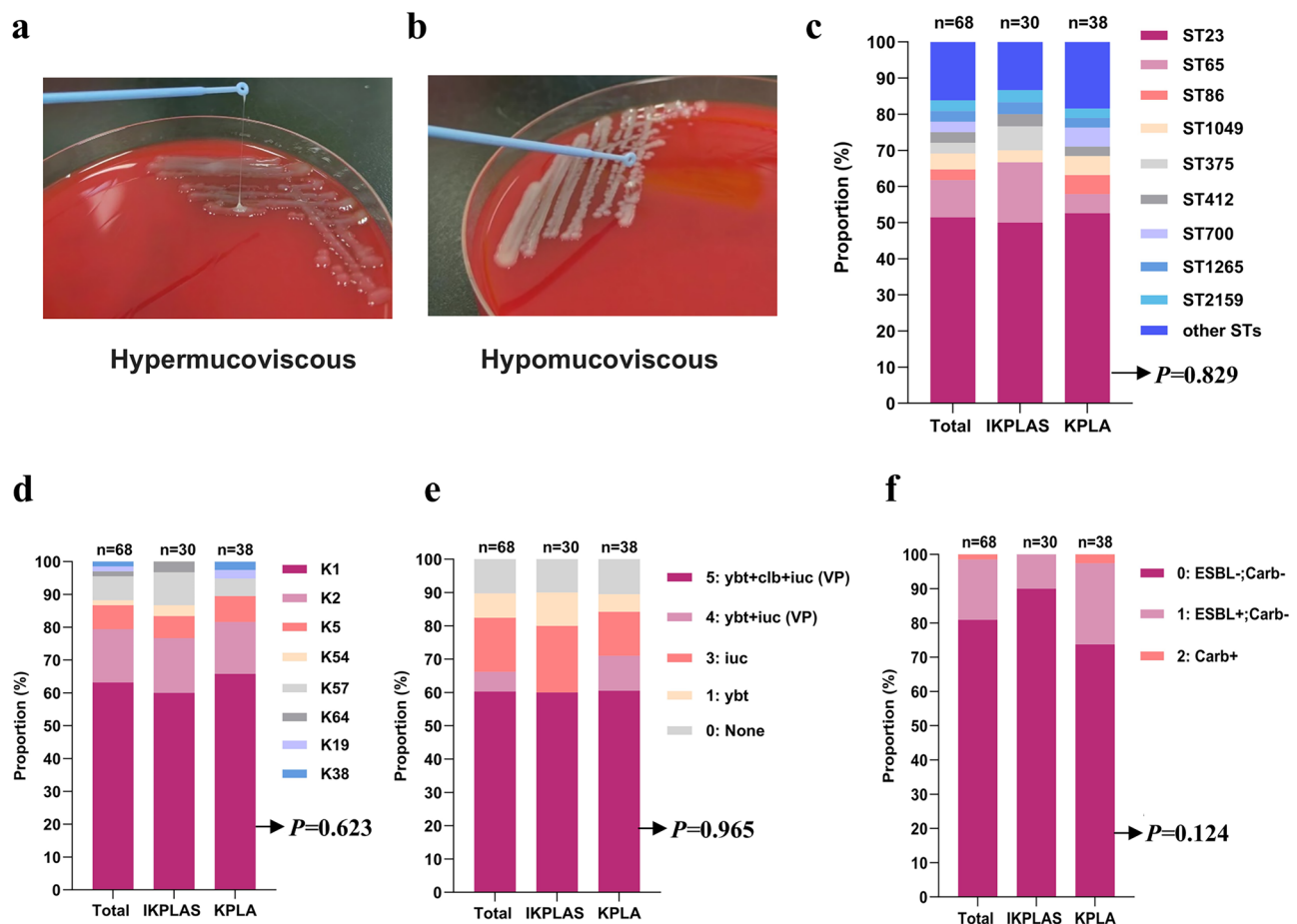


Fig. 1 | Molecular characteristics of *K. pneumoniae* from the IKPLAS and KPLA groups. **a, b** Representative positive and negative string tests of *K. pneumoniae* isolates from the two groups. **c** Percentage of ST clones among *K. pneumoniae* isolates from the IKPLAS and KPLA groups. The nine most common ST types (ST23, ST65, ST86, ST1049, ST375, ST412, ST700, ST1265, ST2159) and other ST types are shown. **d** Percentage of K serotype in *K. pneumoniae* isolates from the IKPLAS and KPLA groups. **e, f** Percentage of virulence (e) and resistance (f) scores in *K.*

pneumoniae from the IKPLAS and KPLA groups. Panels **c–f** were analyzed using a two-sided Pearson's Chi-square test or Fisher's exact test, as appropriate. Virulence and resistance score classifications, as defined by Kleborate, are presented on the right side of (**e, f**). The number of *K. pneumoniae* isolates in each group (*n*) is indicated above. *ybt*, yersiniabactin; *clb*, colibactin; *iuc*, aerobactin; VP, virulence plasmid; ESBL, extended-spectrum β -lactamase; Carb, carbapenemase. Source data are provided as a Source Data file.

observed that isolates cultured in Lac-LB exhibited significantly higher resistance to macrophage phagocytosis compared to those cultured in LB alone (Fig. 3f). The serum resistance assay showed that strains cultured in Lac-LB exhibited increased resistance to serum than those cultured in LB alone, though the difference was not statistically significant (Fig. 3g). Macrophage engulf and digest pathogens, and secrete proinflammatory cytokines, such as interleukin 1 β (IL-1 β), interleukin 6 (IL-6) and tumor necrosis factor- α (TNF α), which are critical for adaptive immunity³⁰. To assess the impact on host immune responses, cytokine expression was measured in RAW264.7 macrophages and corresponding supernatants. Infection with *K. pneumoniae* cultured in Lac-LB led to increased IL-1 β transcription and protein expression, while TNF- α and IL-6 levels remained unchanged (Fig. 3h–k). Collectively, these findings indicated that lactate promotes CPS biosynthesis and enhances the anti-phagocytic properties of *K. pneumoniae*, thereby triggered a stronger inflammatory response.

Lactate enhances *K. pneumoniae* virulence in mice

We next investigated the impact of lactate on *K. pneumoniae* virulence using a mouse LA model (Fig. 4a). Kp9925 is a clinical ST23, K1 serotype isolate, obtained from a patient in the KPLA group. This strain was selected for animal experiments due to its moderate increase in CPS

production in Lac-LB, as shown in Fig. 3a. Survival analysis demonstrated a significantly higher mortality rate in mice infected with Kp9925 cultured in Lac-LB compared to those infected with Kp9925 cultured in LB (Fig. 4b). Further assessment of infection severity showed markedly higher bacterial loads in tissues, elevated levels of inflammatory cytokines, and more severe liver inflammation in mice infected with Kp9925 grown in Lac-LB. This was further supported by larger abscess sizes, elevated serum inflammatory cytokines, more infiltration of neutrophil cells, and pronounced disruption of liver tissue and hepatocyte integrity (Fig. 4c–h). In addition, we evaluated the effect of lactate on the virulence of three additional isolates (Kp9730, Kp9415 and Kp326), which displayed varying degrees of CPS enhancement as shown in Fig. 3a. Survival assays revealed significantly higher mortality rates in mice infected with isolates cultured in Lac-LB compared to those infected with bacteria grown in LB (Supplementary Fig. 4). Together, these findings suggest that lactate-induced virulence enhancement promotes more invasive *K. pneumoniae* infections in mice.

To confirm that lactate enhances *K. pneumoniae* virulence specifically through CPS upregulation in vivo, we constructed a Δ *cps* mutant of Kp9925 by deleting the glycosyltransferase gene *wcaJ*, and compared the virulence of the Δ *cps* mutant cultured in LB and in 40 mM Lac-LB. No significant difference in mortality between mice infected

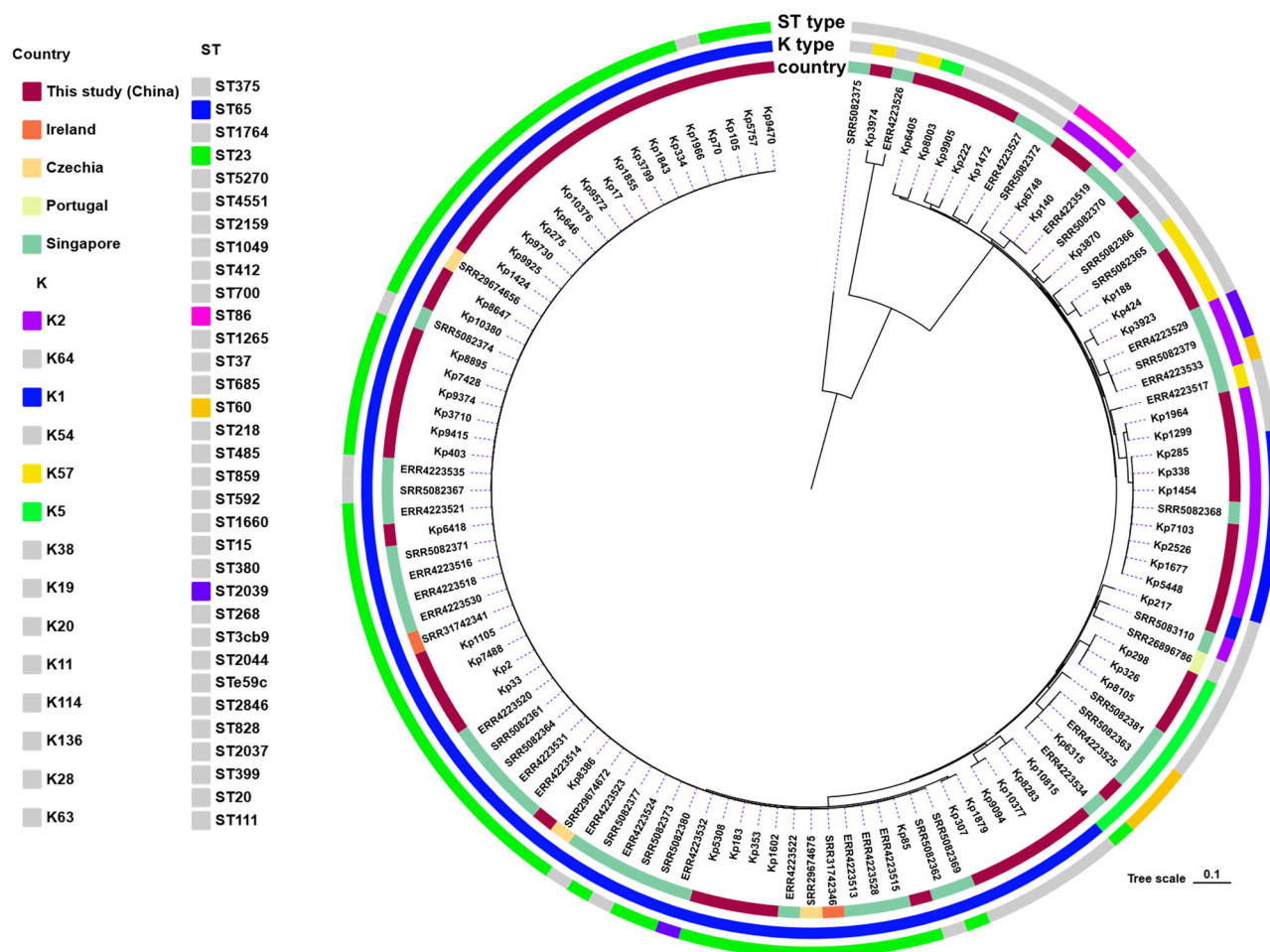


Fig. 2 | The Phylogenetic structure of 117 *K. pneumoniae* isolates responsible for liver abscess. The innermost circle represents the source countries of each isolate. The middle and outermost circles correspond to the K types and ST

types, respectively. In K and ST types, gray block indicated the strain number of certain ST type or K type is less than three. Source data are provided as a Source Data file.

with the Δcps mutant grown in LB and those infected with the mutant grown in Lac-LB was observed (Supplementary Fig. 5). These results suggest that CPS, rather than other virulence factors, is essential for lactate-mediated virulence enhancement in *K. pneumoniae*.

Lactate-induced mannose-specific PTS enzyme II (man-PTS EII) downregulation is associated with increased CPS production

To investigate the molecular mechanisms underlying lactate-induced CPS upregulation, we selected Kp9925 for transcriptomic analysis between culturing in LB and 40 mM Lac-LB. RNA sequencing (RNA-seq) identified 327 differentially expressed genes (DEGs), comprising 155 upregulated and 172 downregulated genes (Fig. 5a). Kyoto Encyclopedia of Genes and Genomes (KEGG) pathway enrichment analysis revealed that a significant proportion of DEGs were linked to PTS systems (Fig. 5b). Among these, the mannose-specific PTS (man-PTS) showed the greatest number of DEGs, including *gfrA*, *gfrB*, *gfrC* and *gfrD*, suggesting a key role of man-PTS in lactate-mediated CPS upregulation (Supplementary Fig. 6). These four genes were downregulated about 5-fold in Kp9925 cultured in Lac-LB compared to LB. To validate these results, we assessed the transcriptional expression of *gfrA*, *gfrB*, *gfrC* and *gfrD* in multiple clinical *K. pneumoniae* isolates using RT-PCR. Consistent with transcriptomic results, the expression of these genes was significantly reduced in clinical *K. pneumoniae* cultured in Lac-LB compared to LB (Fig. 5c).

The PTS systems in *K. pneumoniae* are primarily responsible for sugar transport and phosphorylation. They consist of several

phosphotransferases, including enzyme I (EI), histidine phosphorylated protein (HPr), and the enzyme II (EII) complex³¹. In the man-PTS, EII is composed of EIIA, EIIB, EIIC and EIID which is encoded by *gfrA*, *gfrB*, *gfrC* and *gfrD*, respectively³². Recent studies have suggested that components of the PTS in *K. pneumoniae* can influence CPS production^{33,34}. Based on this evidence, we hypothesize that the lactate-induced man-PTS EII down-regulation may contribute to the increase of CPS biosynthesis.

Man-PTS EII knockout mutant produces more CPS and causes more severe infection in mice than the WT strain

To examine the role of *man-PTS EII* in CPS regulation, we constructed an isogenic $\Delta man-PTS EII$ mutant by deleting the *gfrA-D* genes in Kp9925. Compared to the wild-type (WT) strain, the $\Delta man-PTS EII$ mutant exhibited increased CPS production and upregulation of CPS gene cluster. Complementation with *man-PTS EII* restored CPS production to levels similar to the WT strain. Notably, CPS production and gene expression in the $\Delta man-PTS EII$ mutant did not further increase when cultured in Lac-LB compared to LB alone (Fig. 6a–d). Furthermore, the $\Delta man-PTS EII$ mutant exhibited significantly higher resistance to macrophage phagocytosis than the WT strain. Similar to CPS expression, the anti-phagocytic properties of the $\Delta man-PTS EII$ mutant did not increase further under Lac-LB condition (Fig. 6e). These findings support our hypothesis that *man-PTS EII* mediates the lactate-induced increase in CPS production.

Table 1 | Risk factor analysis of the occurrence of IKPLAS

| Variables | Univariate analysis | | | Multivariate analysis | | |
|----------------------------|---------------------|-------------|--------------|-----------------------|--------------|--------------|
| | OR | 95%CI | P value | OR | 95%CI | P value |
| Demographics | | | | | | |
| Age | 1.040 | 1.002–1.080 | 0.041 | 1.010 | 0.956–1.068 | 0.716 |
| Gender: male | 1.311 | 0.493–3.485 | 0.587 | | | |
| Underlying diseases | | | | | | |
| Diabetes mellitus | 3.651 | 1.266–10.53 | 0.017 | 2.172 | 0.466–10.112 | 0.323 |
| Hypertension | 1.683 | 0.630–4.491 | 0.299 | | | |
| Coronary heart disease | 0.607 | 0.103–3.563 | 0.580 | | | |
| Chronic liver diseases | 2.327 | 0.672–8.060 | 0.183 | | | |
| Chronic kidney diseases | 0.821 | 0.209–3.219 | 0.777 | | | |
| Biliary tract disease | 0.381 | 0.071–2.041 | 0.260 | | | |
| Laboratory test | | | | | | |
| WBC (10 ⁹ /L) | 0.982 | 0.868–1.112 | 0.776 | | | |
| CRP (mg/L) | 1.005 | 0.996–1.013 | 0.278 | | | |
| Neu (%) | 0.998 | 0.963–1.035 | 0.910 | | | |
| Hb (g/L) | 0.990 | 0.965–1.016 | 0.435 | | | |
| AST (U/L) | 1.002 | 0.980–1.025 | 0.843 | | | |
| ALT (U/L) | 1.003 | 0.985–1.021 | 0.747 | | | |
| HbA1c | 1.527 | 1.054–2.211 | 0.025 | | | |
| PCT (ng/mL) | 1.014 | 0.971–1.058 | 0.529 | | | |
| Lactate (mmol/L) | 3.210 | 1.485–6.937 | 0.003 | 4.547 | 1.488–13.89 | 0.008 |
| PT (s) | 0.938 | 0.621–1.418 | 0.761 | | | |
| APTT (s) | 1.003 | 0.896–1.123 | 0.955 | | | |
| Abscess size (cm) | 1.138 | 0.926–1.399 | 0.219 | | | |
| Medical history | | | | | | |
| Cephalosporins | 4th gen | 0.571 | 0.217–1.503 | 0.256 | | |
| Fluoroquinolones | levofloxacin | 0.797 | 0.290–2.188 | 0.660 | | |
| | moxifloxacin | 0.137 | 0.035–0.531 | 0.004 | 0.087 | 0.009–0.875 |
| Carbapenems | imipenem | 0.496 | 0.136–1.803 | 0.287 | | |
| | meropenem | 0.607 | 0.103–3.563 | 0.580 | | |
| Metronidazole | | 0.431 | 0.120–1.544 | 0.196 | | |
| Cephameycins | | 1.795 | 0.369–8.719 | 0.468 | | |
| Aztreonam | | 0.733 | 0.161–3.350 | 0.689 | | |
| Number of puncture | | 3.511 | 1.406–8.770 | 0.007 | 3.050 | 1.172–7.937 |
| length of stay | | 1.028 | 0.981–1.077 | 0.247 | | |

Bolded P values indicate statistically significant differences ($P < 0.05$).

We then employed a mouse LA model to compare the virulence of the WT strain and $\Delta man\text{-}PTS\ EII$ mutant. Mice infected with the $\Delta man\text{-}PTS\ EII$ mutant exhibited markedly higher bacterial loads in tissues, elevated serum IL-6 levels and more severe liver inflammation (Fig. 6f–k). Moreover, survival analysis revealed significantly higher mortality rates in the mice infected with $\Delta man\text{-}PTS\ EII$ mutant compared to those infected with the WT strain (Fig. 6l). These results suggested that lactate-induced downregulation of $man\text{-}PTS\ EII$ enhanced the virulence of *K. pneumoniae*.

Downregulation of $man\text{-}PTS\ EII$ enhances CPS biosynthesis via the cAMP-CRP regulon

Previous studies have established that phosphorylation of PTS components, such as EIIA^{Glc}, can influence cAMP levels by activating adenylate cyclase (AC)³⁵. We hypothesized that lactate-induced $man\text{-}PTS\ EII$ downregulation reduces intracellular cAMP levels, thereby promoting CPS production. To test this, we measured intracellular cAMP levels in the WT strain, $\Delta man\text{-}PTS\ EII$ mutant and complemented (C- $\Delta man\text{-}PTS\ EII$) strains when cultured in LB and Lac-LB. The WT strain showed significantly reduced cAMP levels when grown in Lac-LB

compared to LB alone. Notably, the $\Delta man\text{-}PTS\ EII$ mutant exhibited even lower cAMP levels than both the WT and complemented strains, and cAMP levels in the mutant were not further decreased under Lac-LB conditions (Fig. 7a).

To further elucidate the role of cAMP in regulating CPS production and HMV, we cultured 10 clinical isolates in Lac-LB supplemented with exogenous 0.5 mM cAMP, a concentration previously shown to inhibit glucose-induced CPS production³⁶. Exogenous cAMP significantly inhibited the lactate-induced CPS production and HMV in the 10 clinical isolates (Fig. 7b, c). As cAMP acts through the cAMP receptor protein (CRP), a known negative regulator of CPS biosynthesis³⁷. We next investigated the role of CRP in lactate-induced CPS upregulation by constructing a *crp* knockout (Δcrp) mutant. Compared to the WT strain, the Δcrp mutant exhibited significantly increased CPS production and upregulation of the CPS genes cluster. However, culturing the Δcrp mutant in Lac-LB did not further increase CPS production or genes expression compared to culturing in LB alone (Fig. 7d, e). These results suggested that lactate-induced $man\text{-}PTS\ EII$ downregulation enhanced CPS biosynthesis via suppression of the cAMP-CRP regulon.

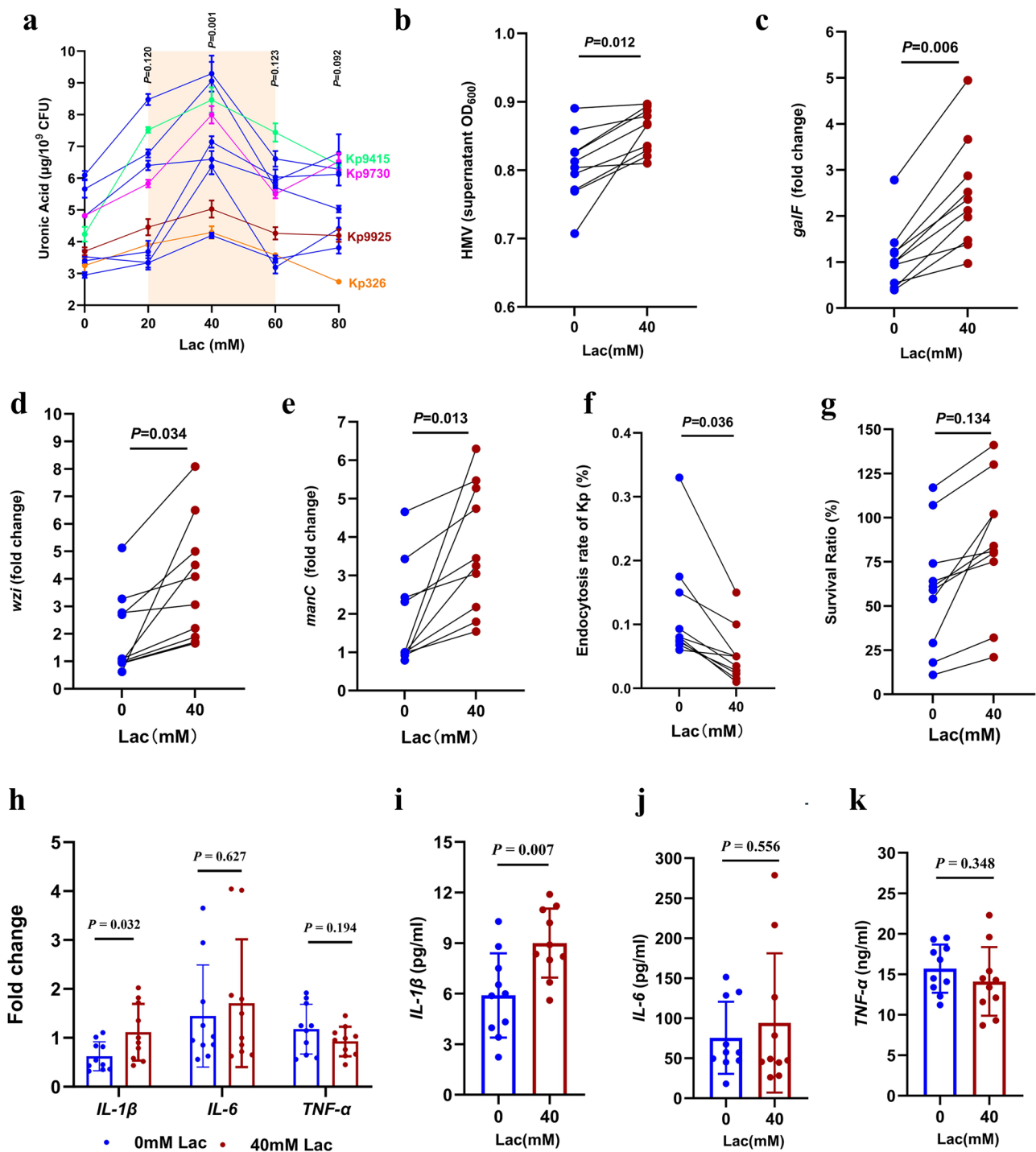


Fig. 3 | Lactate promotes the CPS production in clinical *K. pneumoniae* isolates.

a CPS quantification of 10 clinical *K. pneumoniae* isolates cultured in LB with increasing concentrations of sodium lactate. *P* values comparing each group to the control (0 mM lactate) are shown above the respective groups. The Kp9925 (highlighted in red) was used for RNA-seq and further mechanism investigation, while Kp9730 isolate (purple), Kp9415 (green) and Kp326 (yellow) were used in further animal experiments. **b** HMV of the 10 clinical *K. pneumoniae* isolates cultured in LB and Lac-LB. **c–e** RT-PCR analysis of CPS genes expression in the 10 clinical isolates cultured in LB and Lac-LB. Fold changes are relative to a randomly selected isolate cultured in LB alone. **f** Endocytosis rate of the 10 clinical *K. pneumoniae* isolates by RAW 264.7 macrophages. Data represents the ratio of intracellular bacterial CFU to the input bacteria CFU. **g** Serum resistance assays of 10 clinical *K. pneumoniae* isolates. Percent survival was determined as the number of surviving bacteria relative to the initial bacterial addition. **h** Transcriptional

expression of proinflammatory cytokines in the RAW 264.7 macrophages infected with 10 clinical *K. pneumoniae*. **i–k** ELISA assays measuring proinflammatory cytokines in the supernatant of RAW 264.7 Macrophages infected with 10 clinical *K. pneumoniae*. For panels (**h–k**) *K. pneumoniae* isolates were cultured in LB and Lac-LB for 16 h, washed three times with PBS, and then used to infect RAW 264.7 cells. After 1 h of infection, extracellular bacteria were removed, followed by an additional 2 h of incubation for panel **h**, and 23 h for panels (**i–k**). The transcriptional levels of cytokines in RAW 264.7 cells and protein levels in the supernatant of *K. pneumoniae*-infected RAW 264.7 cells were then measured. Statistical analysis for panels (**a–k**) was performed using a two-sided independent-samples *t*-test. In panels (**a**, **h–k**), error bars show the mean \pm SD. In panels (**b–g**), Each point represents the mean value of three biological replicates for each strain. All experiments were independently repeated three times with similar results. Source data are provided as a Source Data file.

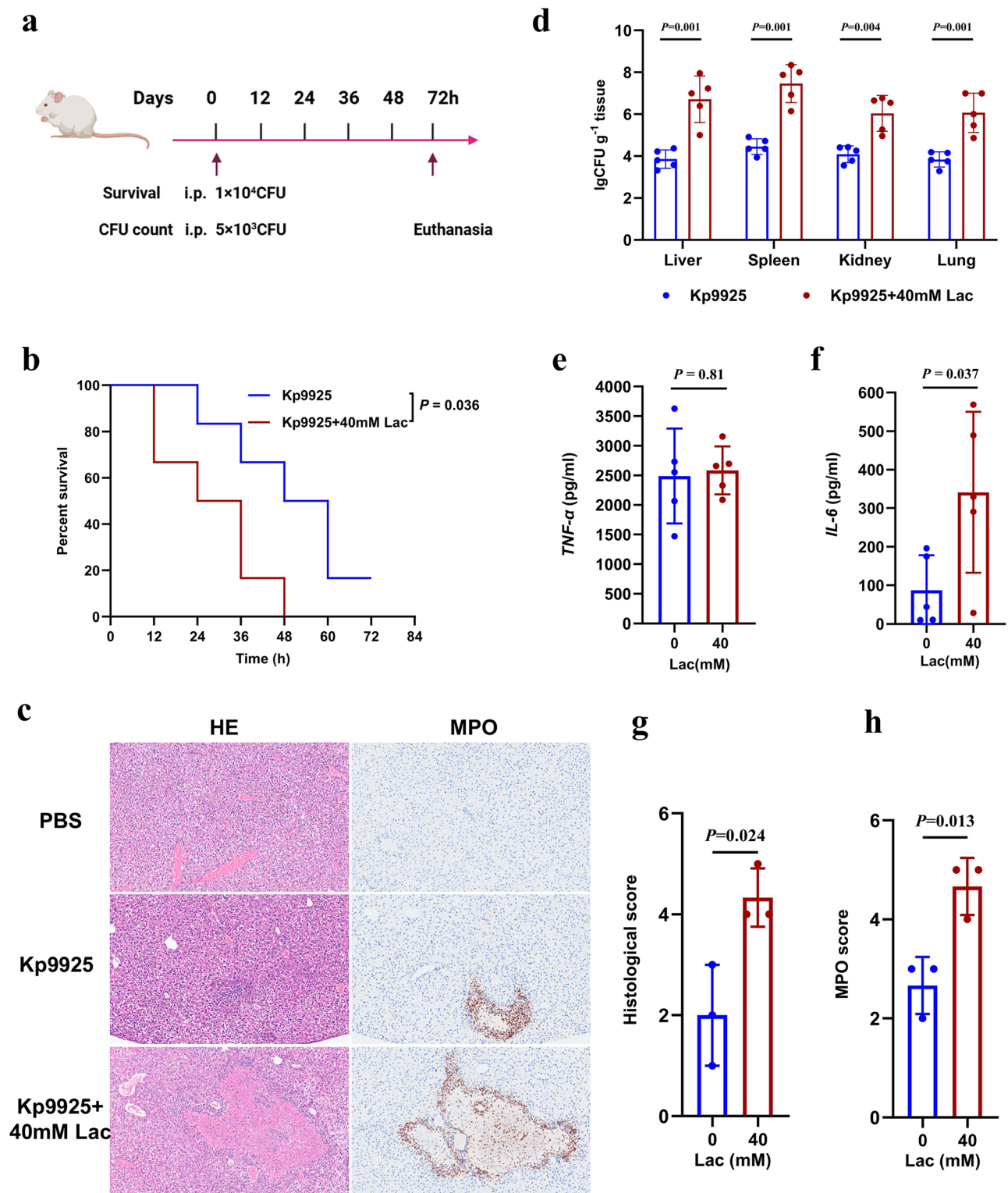


Fig. 4 | Lactate enhances *K. pneumoniae* virulence in mice. **a** Mouse model of liver abscess. For the survival experiment, mice were intraperitoneally injected with 1×10^4 CFU of *K. pneumoniae*. For bacterial load analysis in tissues, mice were received 5×10^3 CFU via intraperitoneal injection. **b** Survival curves of mice infected with Kp9925 cultured in LB or Lac-LB. Mice ($n = 6$ /group) were monitored for 3 days. Statistical analysis was performed using the log-rank tests. **c** Representative histopathology of liver tissues (Hematoxylin-eosin and MPO staining). Images were shown at 200 \times magnification. **d** Bacterial load in the liver, spleen, kidney and lung tissues of mice ($n = 5$ /group). **e–f** Serum levels of proinflammatory cytokines (IL-6

and TNF- α) measured by ELISA in mice infected with Kp9925 cultured in LB or Lac-LB ($n = 5$ /group). **g** Histological scores ($n = 3$ /group). **h** MPO scores ($n = 3$ /group). For panels **g** and **h**, two tissue sections per sample were scored on a 0 to 3 scale, and the cumulative lesion score was obtained by summing the individual scores. For panels **d–h**, n represents the number of biological replicates and statistical analysis was conducted using a two-sided independent-samples *t*-test. Error bars represent the mean \pm SD. All experiments were independently repeated three times with similar results. Source data are provided as a Source Data file.

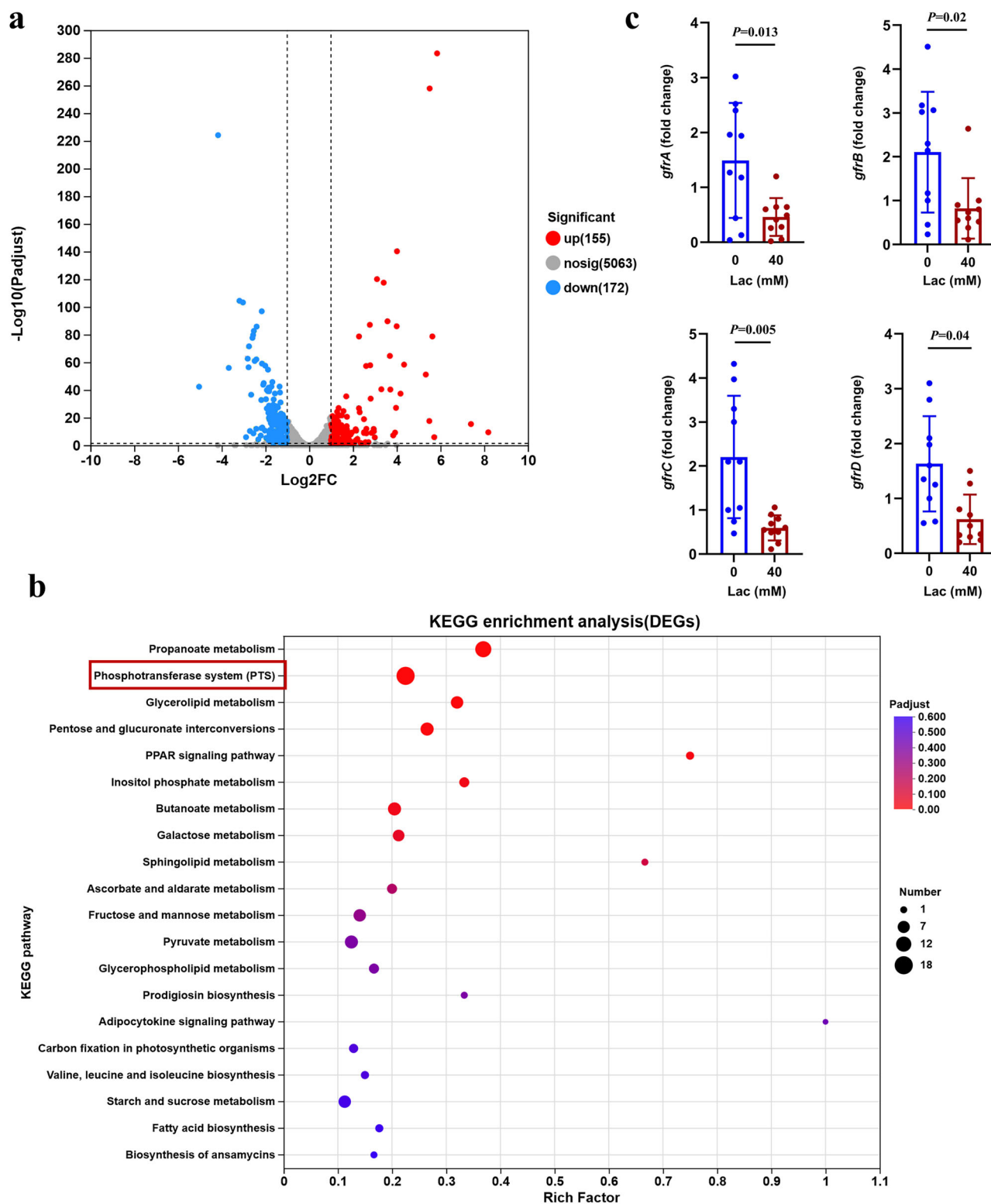


Fig. 5 | Lactate induces transcriptome sequencing and differential gene analysis in *K. pneumoniae*. **a** Volcano map showing differentially expressed genes in Kp9925 cultured in LB versus Lac-LB. **b** KEGG pathway enrichment analysis of differentially expressed genes. **c** Validation of *gfrA*, *gfrB*, *gfrC* and *gfrD* expression in

10 *K. pneumoniae* isolates cultured in LB and Lac-LB. For **(a, b)** Fisher's exact test was used to test significance and adjusted by Benjamini and Hochberg. For panel **c**, statistical analysis was conducted using a two-sided independent-samples *t*-test. Error bars represent the mean \pm SD. Source data are provided as a Source Data file.

Discussion

In recent years, the global incidence of IKPLAS has risen significantly, often leading to severe clinical outcomes^{6–12}. While both host and microbial factors have been implicated in the pathogenesis of the invasive infections^{21,23}, the precise molecular mechanisms remain

poorly understood. Our study bridges this gap by investigating both microbial and host factors in patients with KPLA and IKPLAS. Contrary to previous assumptions, we found no significant differences in the molecular characteristics of *K. pneumoniae* isolates between the two groups. However, elevated blood lactate level was observed as a

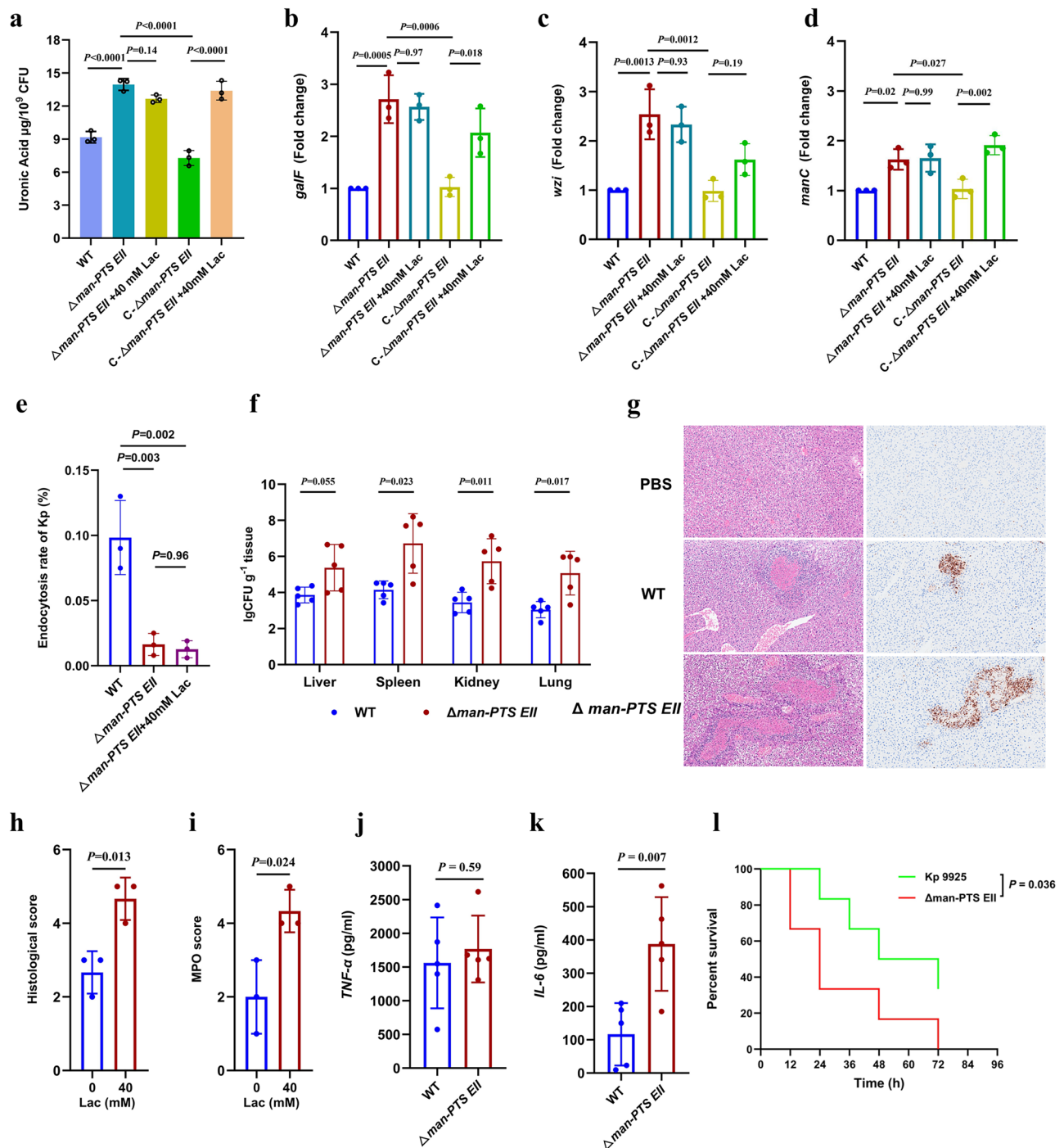


Fig. 6 | *Man-PTS EII* knockout mutant produces more CPS and induces more severe infection in mice compared to the WT strain. **a** CPS quantification of the wild type (WT), $\Delta\text{man-PTS EII}$ mutant and complemented mutant ($\text{C-}\Delta\text{man-PTS EII}$) strains cultured in LB or Lac-LB. **b–d** RT-PCR analysis of CPS encoding genes expression (*galF*, *wzi* and *manC*) in the WT, $\Delta\text{man-PTS EII}$ mutant and $\text{C-}\Delta\text{man-PTS EII}$ strains cultured in LB and Lac-LB. **e** Endocytosis rate of the WT and $\Delta\text{man-PTS EII}$ strains by RAW 264.7 macrophages. Data represent the ratio of intracellular bacterial CFU to the input bacteria CFU. **f** Bacterial loads in liver, spleen, kidney and lung tissues. $n = 5/\text{group}$. **g** Representative histopathology of liver tissues (Hematoxylin-eosin and MPO staining). Images captured at 200 \times magnification. **h, i** Histological and MPO score ($n = 3/\text{group}$). Two tissue sections per sample were

scored on a 0 to 3 scale, and cumulative lesion scores were calculated by summing the individual section scores. **j–k** Serum protein levels of proinflammatory cytokines IL-6 and TNF- α in mice infected with the WT and $\Delta\text{man-PTS EII}$ strains, measured by ELISA. $n = 5/\text{group}$. **l** Survival curves of mice infected with the WT and $\Delta\text{man-PTS EII}$ strains. Mice ($n = 6/\text{group}$) were intraperitoneally injected with 1×10^4 CFU bacteria and monitored for 3 days. Statistical analysis for panels **a–e** was performed using one-way ANOVA with Tukey's post-tests; (**f–k**) were analyzed using two-sided independent-samples *t*-test. The survival analysis (**l**) was performed using the log-rank test. Error bars show the mean \pm SD. n indicates the number of biological replicates for all experiments. Source data are provided as a Source Data file.

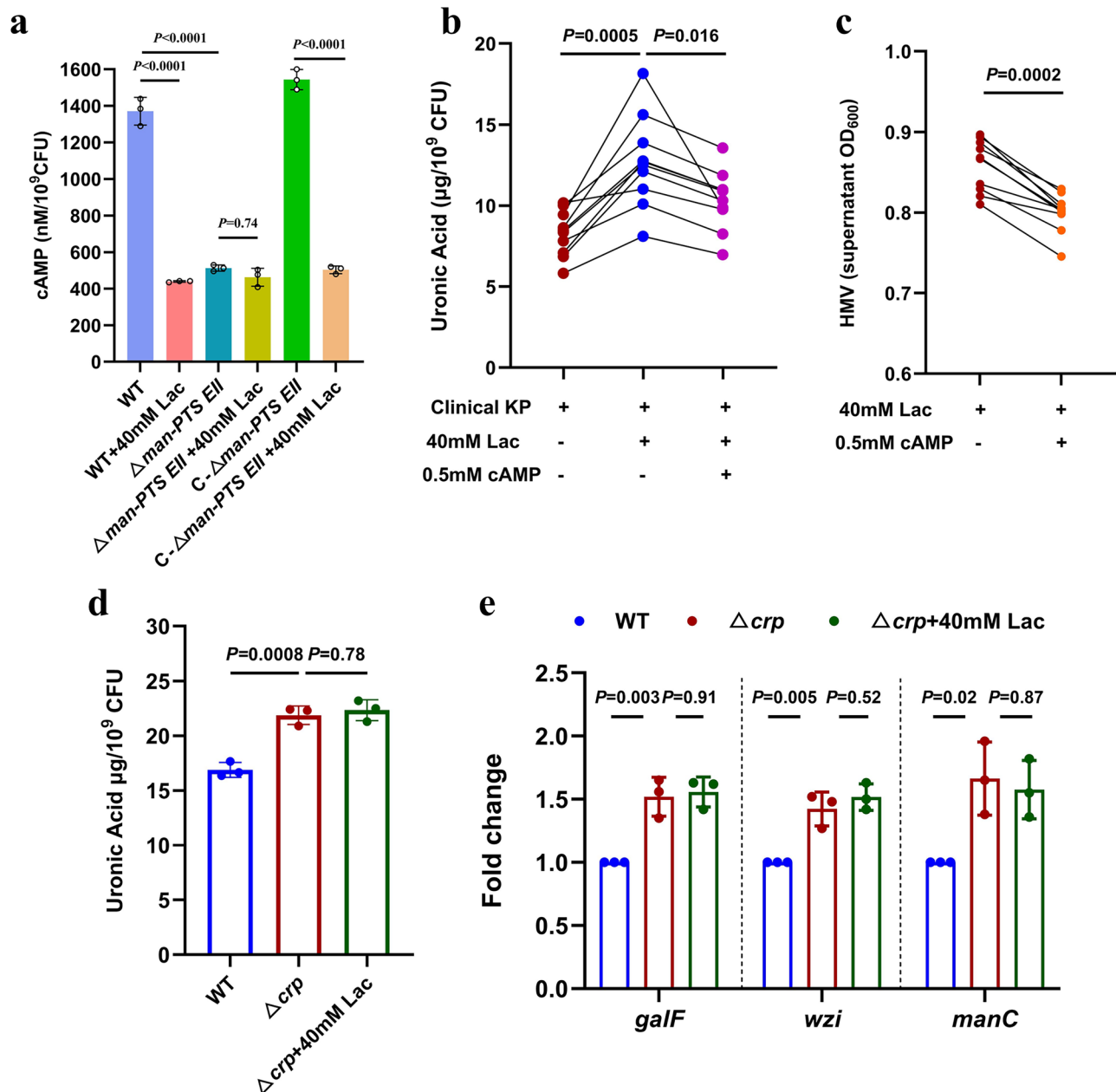


Fig. 7 | Downregulation of Man-PTS EII increases CPS biosynthesis via the cAMP-CRP regulon. a Intracellular cAMP concentration in the wild-type (WT), Δ man-PTS EII mutant, and complemented mutant (C- Δ man-PTS EII) strains cultured in LB or Lac-LB ($n = 3$). **b** CPS quantification of the 10 clinical *K. pneumoniae* isolates grown in LB broth supplemented with lactate and/or cAMP. **c** HMV of the same 10 isolates cultured in Lac-LB with or without cAMP supplementation. **d** CPS quantification of the WT and Δ crp strains in LB or Lac-LB ($n = 3$). **e** Transcriptional expression of CPS gene

cluster in the WT and Δ crp strains cultured in LB or Lac-LB ($n = 3$). the isolates used in panels **b** and **c** are the same as those shown in Fig. 3a. n indicates the number of biological replicates for all experiments. Statistical analysis in (**c**) was performed using a two-sided independent-samples *t*-test, while other panels were analyzed by one-way ANOVA with Tukey's post-tests. In panels (**a**, **d**, **e**), error bars show the mean \pm SD. In panels (**b**, **c**), Each point represents the mean value of three biological replicates for each strain. Source data are provided as a Source Data file.

predictor of IKPLAS, highlighting a pivotal role of lactate in these infections.

Lactate is a by-product of cell metabolism, generated at the end of anaerobic glycolysis. Under normal circumstance, lactate is present in blood and tissues at low

concentrations, typically below 2 mM³⁸. In cancer and inflammatory conditions, however, tissue lactate levels are markedly elevated, often many times higher than blood levels. Although blood lactate concentrations may remain normal or slightly elevated, tissue lactate can reach 15–40 mM^{39–42}. In recent years, research on lactate has mainly focused on its immunosuppressive role within the tumor microenvironment. More recently, lactate's involvement in enhancing

bacterial virulence has also gained significant attention. Lactate has been shown to promote the expansion of *Campylobacter jejuni* in the gut, enhance systemic infection in *Salmonella Typhimurium*, and support *Helicobacter pylori* colonization by promoting complement resistance^{25,27,43}. In our study, elevated blood lactate level was identified as an independent risk factor for IKPLAS. Building on these findings, we hypothesized that lactate levels are elevated in the liver abscess microenvironment, where it enhances *K. pneumoniae* virulence by upregulating key virulence factors, thereby driving the progression of IKPLAS. To test this hypothesis, we examined the effect of lactate on virulence factor regulation at varying concentrations. Our results showed that CPS production peaked at 40 mM lactate in clinical *K.*

pneumoniae isolates. Consequently, we focused on lactate's role in CPS regulation at this concentration, which may be relevant to LA conditions. Further investigation revealed that lactate enhanced *K. pneumoniae* virulence in a murine model. Consistent with other studies^{25,27,43}, our results suggest that lactate enhanced the virulence of *K. pneumoniae* by increasing CPS biosynthesis.

Transcriptomic analysis identified significant downregulation of *man-PTS EII* in *K. pneumoniae* exposed to lactate, shedding light on a regulatory mechanism. The PTS system, traditionally associated with carbohydrate transport, also plays a significant role in regulating downstream genes expression. In line with previous studies³³, we found that deletions of *man-PTS EII* in Kp9925 significantly enhanced the production of CPS. The phosphorylation status of PTS components has been shown to directly affect intracellular cAMP levels, which plays global regulation through the CRP³⁵. In our study, we also observed that the lactate-induced downregulation of *man-PTS EII* reduced cAMP levels and consequently increased CPS production in *K. pneumoniae*. This mechanism aligns with previous findings by Ching-Ting Lin et al³⁶, who demonstrated that cAMP reduction in glucose-rich environments similarly enhanced CPS biosynthesis. Our study linked the elevated blood lactate levels with CPS production via PTS-CRP axis, identifying the regulatory pathway of lactate enhancing virulence of *K. pneumoniae*.

A limitation of our study is the inability to measure lactate concentrations in abscess samples from our patient cohort, owing to the retrospective nature of the study. Future research should confirm elevated lactate levels in abscess sample from patients with IKPLAS. Collectively, our results suggest that managing lactate levels may be a critical strategy in reducing mortality rates associated with these invasive infections.

In conclusion, we have demonstrated that lactate promoted the CPS biosynthesis in *K. pneumoniae* isolates, which may be a driver for the progression of IKPLAS. These findings carry important clinical implications, as elevated lactate levels are well-established predictors of poor outcomes in sepsis and other critical illnesses. However, lactate's role in driving bacterial virulence has been largely overlooked. Our study highlights lactate as a key signaling molecule in *K. pneumoniae* pathogenicity and suggests that targeting lactate levels may represent novel therapeutic strategy to improve patients' outcomes in IKPLAS cases.

Methods

Ethics statement

All of our research complies with the relevant ethical regulations. All participants or their legal guardians have provided written informed consent for the use of strains and data for this present study. All patients and data included in the study were anonymized. This study was approved by the Ethics Committee of Renji Hospital, School of Medicine, Shanghai Jiaotong University (LY2024-295-B).

All animal procedures were performed in accordance with the laboratory animal care and use guidelines of the Chinese Association for Laboratory Animal Sciences (CALAS). Approval was obtained from the Ethics Committee of Shanghai Yishang Biotechnology Co (YS-JL-001). Specific pathogen-free (SPF) female BALB/c mice (6 to 8 weeks old) were obtained from Shanghai JieSijie Laboratory Animals Co. Mice were housed at 19–26 °C at a humidity of 40–70% and with a light/dark cycle of 12 h/12 h in-house under SPF conditions with access to autoclaved food, water, and corn cob bedding. Cage changes were performed in a laminar flow hood, accommodating 2–3 mice per cage. Age- and littermate-matched mice were randomly assigned into treatment groups in each experiment. Female mice were used as they are more gentle and less difficult to handle.

Clinical data collection and analysis

From January 2016 to December 2023, a total of 68 patients diagnosed with LA caused by *K. pneumoniae* were enrolled in the study. Clinical data were extracted from electronic medical records and thoroughly

reviewed. Based on whether or not they had extrahepatic invasive infections, patients were divided into IKPLAS and KPLA groups. We compared the two groups in terms of demographics, underlying conditions, laboratory test results, abscess size and location, medical history, number of punctures, and length of hospital stay. Additionally, we assessed the risk factors for IKPLAS using both univariate and multivariate logistic regression analyses.

Isolate collection and antimicrobial susceptibility testing

A total of 68 non-repetitive *K. pneumoniae* isolates were collected from 68 patients with LA caused by *K. pneumoniae*. Of these, 60 isolates were derived from pus samples and 8 from blood cultures. When both pus and blood cultures from the same patient yielded *K. pneumoniae* isolates, the isolate isolated from the pus sample was preferentially selected for further analysis. Bacterial identification was confirmed using matrix-assisted laser desorption/ionization-time of flight mass spectrometry (bioMérieux VITEK MS).

Antimicrobial susceptibility to 14 commonly used antibiotics was evaluated using the broth microdilution method and interpreted based on Clinical and Laboratory Standards Institute (CLSI) guidelines (M100-ED31)⁴⁴. *Escherichia coli* ATCC 25922 and *E. coli* ATCC 35218 were tested as the quality control strains.

HMV phenotype, capsule extraction and uronic acid quantification

The HMV phenotype was evaluated using the string test as previously described⁴⁵. A positive string test was defined by the formation of viscous strings greater than 5 mm in length when a loop was used to stretch the colony on an agar plate. Additionally, the HMV phenotype was quantified using a low-speed centrifugation assay⁴⁶. Briefly, *K. pneumoniae* strains were cultured overnight in 3 ml LB broth at 37 °C. Next, 1 ml of culture was centrifuged for 5 minutes at 1000 × *g*, and the optical density at 600 nm (OD₆₀₀) of the supernatant was measured. Final readings were normalized to the OD₆₀₀ of the input culture before centrifugation. At least three biological replicates were prepared for each isolate.

CPS quantification was performed as previously described with minor modification⁴⁴. Briefly, 500 µl overnight samples were mixed with 1% Zwittergent 3–14 detergent (Merck, catalog number 693017) in 100 mM citric acid (Sangon Biotech, catalog number A610055), and incubated overnight at 50 °C. Uronic acid was then precipitated using ethanol, incubated with sodium tetraborate/sulfuric acid (tetraborate, Sigma-Aldrich, catalog number 221732; sulfuric acid, Sinopharm Chemical Reagent, catalog number 10021608) and boiled for 5 min. Following this, 3-hydroxydi phenol (Sigma-Aldrich, catalog number 262250) was added. The absorbance at 520 nm was measured, and uronic acid were calculated using a standard curve of glucuronic acid. CPS quantification is expressed as microgram per 10⁹ colony forming units (CFU).

Whole-genome sequencing and bioinformatics analysis

Genomic DNA was extracted and purified using the TIANamp Bacterial DNA Kit (TIANGEN Biotech, catalog number DP302) and subsequently sequenced on the HiSeq X Ten PE150 sequencer platform (Illumina, USA), as previously described⁴⁷.

Quality control of the reads was performed using the quality control option in CLC Genomics Workbench 12.0 (QIAGEN, Aarhus, Denmark), and the raw data were filtered prior to assembly. Sequences containing more than 10% ambiguous N bases or shorter than 30 bp were removed. De novo assembly of the filtered data was conducted in CLC Genomics Workbench using the default settings. The generated de novo assembled contigs were then subjected to BLAST searches against the drug resistance gene database and the virulence factors database to identify resistance and virulence gene profiles. STs, capsular serotyping, virulence and resistance genes were determined

using Kleborate²⁴. The presence of *ybt* encoding yersiniabactin, *clb* encoding colibactin and *iuc* encoding aerobactin are used to assign a virulence score, while Extended-Spectrum β -Lactamases (ESBLs), carbapenemase and colistin resistance are used to calculate resistance scores as follows previously describe²⁴.

Phylogenetic analysis

We compared the 68 genomes sequenced in this study with 49 published genomes of *K. pneumoniae* isolated from LA, retrieved from the SRA database. SNP calling and phylogenetic analysis were performed using CLC Genomics Workbench 12.0 with default settings. The NTUHK2044 genome (GCF_000009885.1) served as the reference for read mapping. A maximum likelihood tree was constructed in CLC Genomics Workbench 12.0 using the General Time Reversible (GTR) model of nucleotide substitution, incorporating among-site rate heterogeneity across four categories (GTR + Γ). The tree was then annotated using ChiPlot⁴⁸.

Quantitative RT-PCR

Total RNA from the bacteria was extracted using the RNeasy® Mini Kit (Qiagen, catalog number 74104) following the manufacturer's instructions. The purity and concentration of the RNA were assessed with a NanoDrop spectrophotometer (Thermo Scientific). A total of 1 μ g RNA was reverse-transcribed into complementary DNA using the PrimeScript™ RT reagent Kit with gDNA Eraser (Takara, catalog number RR047Q). Real-time PCR was conducted using the 7500 real-time PCR system (Applied Biosystems). Transcription expression of *galF*, *wzi*, *manC*, *gfrA*, *gfrB*, *gfrC* and *gfrD* were detected. Each reaction was performed in triplicate, and gene expression levels were calculated by the $2^{-\Delta\Delta CT}$ method using *23S rRNA* as a reference. Primers for quantitative RT-PCR are listed in Supplementary Data files.

Macrophage phagocytosis assay

The phagocytosis assay was performed using the mouse macrophage cell line RAW 264.7 (ATCC catalog number TIB-71), as previously described³³. Briefly, bacteria cultured in LB and Lac-LB were washed three times with phosphate-buffered saline (PBS) and used to infect cells at a multiplicity of infection (MOI) of 50 for 1 h. Notably, lactate was not included in the bacterial and cell culture mixture during the infection process. After infection, cells were washed three times with PBS to remove bacteria. 300 μ g/ml hygromycin (Sangon Biotech, catalog number A600230) was used for 1 h to eliminate extracellular bacteria as previously described^{49,50}. Subsequently, the cells were washed three times with $1\times$ PBS, and treated with 1 ml of 0.25% TritonX-100 (Sangon Biotech, catalog number A110694) for 30 minutes to release the intracellular bacteria. The input and intracellular bacteria were counted by serial dilution and agar plating. The bacterial endocytosis rate was calculated as the ratio of intracellular bacteria CFU to the input bacteria CFU.

Serum resistance assay

Serum resistance activity was measured as previously described, with minor modifications⁵¹. Bacterial suspensions containing 10^6 CFU/ml were collected from mid-log phase cultures, mixed at a 1:3 (vol/vol) ratios with pooled healthy people serum and incubated at 37 °C. Colony counts were obtained for the initial mixture and after 2 h of incubation using the serial dilution method. The survival was expressed as the ratio of CFU counts after 2 h of incubation to the initial CFU count.

Mouse models

Mice LA model was performed as previously described⁵². *K. pneumoniae* was cultured overnight in LB broth, diluted 1:100 into fresh LB or Lac-LB and allowed to grow to the logarithmic phase. After centrifugation at $12,000\times g$ for 5 minutes, the bacteria were washed and

resuspended in $1\times$ PBS. To assess survival, mice were intraperitoneally injected with 1×10^4 CFU *K. pneumoniae* and monitored for up to three days post-injection. For tissue CFU counting, mice were intraperitoneally injected with 5×10^3 CFU *K. pneumoniae*. Two days after infection, the mice were euthanized, and the liver, spleen, kidney, lung and blood were collected for further analysis. The number of mice used in each experiment is indicated in the figure legends. No mice or data points were excluded from the analyses.

Analysis of the bacterial burden

We used serial dilution and agar plating to perform tissue bacteria loads. Briefly, tissue samples were weighed and collected in 2 ml Eppendorf tubes containing pre-cooled PBS. The samples were homogenized for 2 minutes using a grinder, followed by serial dilution and plating on LB agar plates. The colony was counted and calculated as CFU per gram of tissue.

Histopathological analysis

Formalin-fixed, paraffin-embedded liver tissue segments were processed for hematoxylin and eosin (H&E) staining and myeloperoxidase (MPO) staining. H&E staining was used to evaluate liver abscess formation and necrosis, while MPO staining, with the commercial MPO antibody (Abcam, catalog number ab208670, 1:1000), was employed as a marker for neutrophil influx, as MPO is predominantly expressed by polymorphonuclear leukocytes (PMNs). Slides were independently examined by a histopathologist who was blinded to the treatment conditions. Two tissue sections from each sample were scored on a scale of 0 to 3, and the cumulative lesion score was calculated as the sum of these individual scores. The Enhance-labeled polymer system (ELPS, EnVision, DAKO) was used to detect MPO expression.

Enzyme-linked immunosorbent assay (ELISA) assays

The ELISA assays for IL-6, TNF- α and IL-1 β were performed by collecting the supernatant from *K. pneumoniae*-infected RAW 264.7 cells after 1 h of infection, followed by an additional 23 h of incubation. Serum samples from mice infected with *K. pneumoniae* were also collected and used for ELISA assays. The assays were conducted according to the manufacturer's instructions using the following ELISA kits: Mouse IL-6 ELISA (Absin, catalog number abs520004-96T), Mouse TNF- α ELISA (Absin, catalog number abs520010-96T) and Mouse IL-1 β ELISA kit (Absin, catalog number abs520001-96T).

RNA sequencing

RNA sequencing was conducted in triplicate to investigate the regulatory mechanism of lactate on CPS. Kp9925 cultured in LB and Lac-LB were grown to an OD₆₀₀ of 0.6. Total RNA was extracted and purified using the RNeasy® Mini Kit (Qiagen, catalog number 74104) and subjected to 150 bp paired-end sequencing on the Illumina NovaSeq platform. The Majorbio Cloud Platform (www.majorbio.com) was used for data analysis⁵³. Raw data were filtered using SeqPrep v1.2 (available at <https://github.com/jstjohn/SeqPrep>) and Sickle v1.33 (available at <https://github.com/najoshi/sickle>) with default settings. High-quality reads from each sample were aligned to the reference assemblies of Kp9925 using Bowtie 2 v2.5.2 with default parameters⁵⁴. Quantitative analysis of gene expression was performed using RSEM v1.3.3⁵⁵ and standardized by transcripts per million (TPM). Differential gene expression analysis was conducted using the DESeq2 v3.18⁵⁶ package. Kyoto Encyclopedia of Genes and Genomes (KEGG) pathway analysis was employed to identify enriched functions and pathways of differentially expressed genes (DEGs). KEGG pathways were assessed for statistical significance using Fisher's exact test with Goatools v1.3.1⁵⁷ and KOBAS 2.0⁵⁸. The false discovery rate (FDR) correction, implemented by the Benjamini-Hochberg (BH) method, was performed to minimize Type I errors.

Deletion clones and complementation

The Kp9925 Δ man-PTS *EII* (Δ gfrA-D), Δ crp and Δ cps (Δ wcaJ) mutants were constructed using homologous recombination, as previously described⁵⁹. Briefly, two DNA fragments, each ~500 bp long and flanking the target deletion region, were cloned into the pCONJ6H vector, which contains a counter-selectable marker (*sacB* gene) and a hygromycin resistance gene, via gibsion. This resulting plasmid was then mobilized from *E. coli* MFDpir to Kp9925 via conjugation. Transconjugants, where the plasmid integrated into the chromosome through homologous recombination, were selected on LB agar plates containing 300 μ g/ml hygromycin. Several colonies were subsequently cultured in LB broth supplemented with 300 μ g/ml of hygromycin until reaching the log phase at 37 °C. Afterward, these cultures were spread onto LB agar plates containing 10% sucrose for further selection. The deletion of the genes was confirmed using PCR and sequencing.

For the complementation of the deletion mutants, the man-PTS *EII*, *crp* and *wcaJ* genes from Kp9925 were individually amplified and cloned into the pHSG396 vector (Takara). The recombinant plasmids were then introduced into the corresponding man-PTS *EII*, *crp* and *wcaJ* mutant strains by transformation. Mutants were selected on LB agar plates containing chloramphenicol. Gene expression was driven by the promoter included in the pHSG396 vector.

Detection of cAMP

The detection of cAMP was performed as previously described⁶⁰. Briefly, bacterial suspension was adjusted to 1×10^9 CFU/ml and washed twice in PBS. Then, the bacteria were resuspended in 300 μ l 1X lysis buffer and lysated by sonication. The lysate was centrifuged briefly at $12,000 \times g$ for 10 min, and the supernatant was tested for cAMP levels by using cAMP Assay (USA R&D Systems, Inc. catalog number KGE002B) according to manufacturer's recommendations.

Statistics

Statistical analysis was performed using SPSS 26.0 (IBM Corp., Armonk, NY, USA). Continuous data were compared using the independent-samples *t*-test while the chi-square test was used to compare categorical data. Univariate analysis was used in risk factor evaluation for each variable. Variables with a *P* value of less than 0.05 were added in the multivariate logistic regression model to identify the risk factors associated with IKPLAS. Analyses of three or more groups were performed using one-way ANOVA. Survival curves were analysed by log-rank test. A two-sided *P* value of < 0.05 was considered statistically significant.

Reporting summary

Further information on research design is available in the Nature Portfolio Reporting Summary linked to this article.

Data availability

All data needed to evaluate the conclusions are present in the paper or the supplementary material. Genome sequences and the RNA sequence data used in this study have been deposited in the National Center for Biotechnological Information (NCBI) database (Genome data, BioProject number: PRJNA1180191 <http://www.ncbi.nlm.nih.gov/bioproject/1180191>; RNA sequence data, BioProject numbers: PRJNA1180297 <http://www.ncbi.nlm.nih.gov/bioproject/1180297>). Source data are provided with this paper.

References

1. Siu, L. K., Yeh, K.-M., Lin, J.-C., Fung, C.-P. & Chang, F.-Y. *Klebsiella pneumoniae* liver abscess: a new invasive syndrome. *Lancet Infect. Dis.* **12**, 881–887 (2012).
2. Lin, Y. et al. Clinical characteristics of pyogenic liver abscess with and without biliary surgery history: a retrospective single-center experience. *BMC Infect. Dis.* **24**, 479 (2024).
3. Li, W., Chen, H., Wu, S. & Peng, J. A comparison of pyogenic liver abscess in patients with or without diabetes: a retrospective study of 246 cases. *BMC Gastroenterol.* **18**, 144 (2018).
4. Song, H., Wang, X., Lian, Y. & Wan, T. Analysis of the clinical characteristics of 202 patients with liver abscess associated with diabetes mellitus and biliary tract disease. *J. Int. Med. Res.* **48**, 300060520949404 (2020).
5. Zhang, J. et al. Clinical features and prognosis of gas-forming and non-gas-forming pyogenic liver abscess: a comparative study. *Surg. Infect. (Larchmt.)* **22**, 427–433 (2021).
6. Zhang, Z., Wang, H., Guo, Y., Liu, Z. & Chang, Z. Metagenome analysis of the bacterial characteristics in invasive *Klebsiella pneumoniae* liver abscesses. *Front Cell Infect. Microbiol.* **12**, 812542 (2022).
7. Chen, C. E. & Shih, Y. C. Monomicrobial *Klebsiella pneumoniae* necrotizing fasciitis with liver abscess: a case report and literature review. *Ann. Plast. Surg.* **78**, S28–S31 (2017).
8. Shin, S. U. et al. Clinical and radiological features of invasive *Klebsiella pneumoniae* liver abscess syndrome. *Acta Radio.* **54**, 557–563 (2013).
9. Kinoshita, O. et al. *Klebsiella* invasive liver abscess syndrome presenting with a central nervous system manifestation secondary to latent cholecystitis: a case report. *J. Med Case Rep.* **16**, 234 (2022).
10. Zou, Q. & Li, Y. Hypervirulent *Klebsiella pneumoniae*. *N. Engl. J. Med.* **385**, 833 (2021).
11. Wakabayashi, S. I. et al. Invasive liver abscess syndrome accompanied by spondylodiscitis: a case report and review of the literature. *Clin. J. Gastroenterol.* **13**, 927–934 (2020).
12. Gupta, A., Bhatti, S., Leytin, A. & Epelbaum, O. Novel complication of an emerging disease: Invasive *Klebsiella pneumoniae* liver abscess syndrome as a cause of acute respiratory distress syndrome. *Clin. Pr.* **8**, 1021 (2017).
13. Zhu, J., Wang, T., Chen, L. & Du, H. Virulence Factors in Hypervirulent *Klebsiella pneumoniae*. *Front Microbiol.* **12**, 642484 (2021).
14. Walker, K. A. & Miller, V. L. The intersection of capsule gene expression, hypermucoviscosity and hypervirulence in *Klebsiella pneumoniae*. *Curr. Opin. Microbiol.* **54**, 95–102 (2020).
15. Paczosa, M. K. & Meccas, J. *Klebsiella pneumoniae*: going on the offense with a strong defense. *Microbiol. Mol. Biol. Rev.* **80**, 629–661 (2016).
16. Liu, S. et al. Effects of aerobactin-encoding gene *iucB* and regulator of mucoid phenotype *rmpA* on the virulence of *Klebsiella pneumoniae* causing liver abscess. *Front Cell Infect. Microbiol.* **12**, 968955 (2022).
17. Gan, L. et al. Genetic diversity and pathogenic features in *Klebsiella pneumoniae* isolates from patients with pyogenic liver abscess and pneumonia. *Microbiol. Spectr.* **10**, e0264621 (2022).
18. Liu, J. et al. Characteristics of *Klebsiella pneumoniae* pyogenic liver abscess from 2010–2021 in a tertiary teaching hospital of South China. *J. Glob. Antimicrob. Resist.* **36**, 210–216 (2024).
19. Yin, D. et al. Clinical characteristics and management of 1572 patients with pyogenic liver abscess: A 12-year retrospective study. *Liver Int.* **41**, 810–818 (2021).
20. Liu, Y., Zhu, H., Yin, Y. & Yan, Z. Left eye enucleation caused by multi-systemic *Klebsiella pneumoniae* invasive syndrome. *J. Int Med Res.* **50**, 3000605211069284 (2022).
21. Fung, C.-P. et al. A global emerging disease of *Klebsiella pneumoniae* liver abscess: is serotype K1 an important factor for complicated endophthalmitis?. *Gut* **50**, 420–424 (2002).
22. Babouee et al. First two cases of severe multifocal infections caused by *Klebsiella pneumoniae* in Switzerland: characterization of an atypical non-K1/K2-serotype strain causing liver abscess and endocarditis. *J. Glob. Antimicrob. Resist.* **10**, 165–170 (2017).
23. Wang, H., Guo, Y., Liu, Z. & Chang, Z. The type VI secretion system contributes to the invasiveness of liver abscess caused by *Klebsiella pneumoniae*. *J. Infect. Dis.* **228**, 1127–1136 (2023).

24. Lam, M. M. C. et al. A genomic surveillance framework and genotyping tool for *Klebsiella pneumoniae* and its related species complex. *Nat. Commun.* **12**, 4188 (2021).
25. Sinha, R. et al. Gut metabolite L-lactate supports *Campylobacter jejuni* population expansion during acute infection. *Proc. Natl. Acad. Sci. USA* **121**, e2316540120 (2024).
26. Wang, Y. et al. Post-translational toxin modification by lactate controls *Staphylococcus aureus* virulence. *Nat. Commun.* **15**, 9835 (2024).
27. Hu, S. & Ottemann, K. M. *Helicobacter pylori* initiates successful gastric colonization by utilizing L-lactate to promote complement resistance. *Nat. Commun.* **14**, 1695 (2023).
28. Jiang, T., Gao, C., Ma, C. & Xu, P. Microbial lactate utilization: enzymes, pathogenesis, and regulation. *Trends Microbiol.* **22**, 589–599 (2014).
29. Opoku-Temeng, C., Kobayashi, S. D. & DeLeo, F. R. *Klebsiella pneumoniae* capsule polysaccharide as a target for therapeutics and vaccines. *Comput. Struct. Biotechnol. J.* **17**, 1360–1366 (2019).
30. Asgari, F. et al. The Long Pentraxin PTX3 Controls *Klebsiella pneumoniae* Severe Infection. *Front. Immunol.* **12**, 666198 (2021).
31. Postma, P. W., Lengeler, J. W. & Jacobson, G. R. Phosphoenolpyruvate: carbohydrate phosphotransferase systems of bacteria. *Microbiol. Rev.* **57**, 543–594 (1993).
32. Jeckelmann, J. M. & Erni, B. The mannose phosphotransferase system (Man-PTS) - Mannose transporter and receptor for bacteriocins and bacteriophages. *Biochim. Biophys. Acta Biomembr.* **1862**, 183412 (2020).
33. Panjaitan, N. S. D. et al. The PTS components in *Klebsiella pneumoniae* affect bacterial capsular polysaccharide production and macrophage phagocytosis resistance. *Microorganisms* **9**, 335 (2021).
34. Lin, D. et al. The fructose-specific phosphotransferase system of *Klebsiella pneumoniae* is regulated by global regulator CRP and Linked to Virulence and Growth. *Infect. Immun.* **86**, e00340-18 (2018).
35. Parsons, J. B. et al. In-patient evolution of a high-persisters *Escherichia coli* strain with reduced in vivo antibiotic susceptibility. *Proc. Natl. Acad. Sci. USA* **121**, e2314514121 (2024).
36. Lin, C. T. et al. Role of the cAMP-dependent carbon catabolite repression in capsular polysaccharide biosynthesis in *Klebsiella pneumoniae*. *PLoS One* **8**, e54430 (2013).
37. Xu, L., Li, J., Wu, W., Wu, X. & Ren, J. *Klebsiella pneumoniae* capsular polysaccharide: mechanism in regulation of synthesis, virulence, and pathogenicity. *Virulence* **15**, 2439509 (2024).
38. Kraut, J. A. & Madias, N. E. Lactic acidosis: current treatments and future directions. *Am. J. Kidney Dis.* **68**, 473–482 (2016).
39. Colegio, O. R. et al. Functional polarization of tumour-associated macrophages by tumour-derived lactic acid. *Nature* **513**, 559–563 (2014).
40. Hirschhaeuser, F., Sattler, U. G. A. & Mueller-Klieser, W. Lactate: a metabolic key player in cancer. *Cancer Res.* **71**, 6921–6925 (2011).
41. Goetze, K., Walenta, S., Ksiazkiewicz, M., Kunz-Schughart, L. A. & Mueller-Klieser, W. Lactate enhances motility of tumor cells and inhibits monocyte migration and cytokine release. *Int. J. Oncol.* **39**, 453–463 (2011).
42. Walenta, S. et al. High lactate levels predict likelihood of metastases, tumor recurrence, and restricted patient survival in human cervical cancers. *Cancer Res.* **60**, 916–921 (2000).
43. Jiang, L. et al. *Salmonella Typhimurium* reprograms macrophage metabolism via T3SS effector SopE2 to promote intracellular replication and virulence. *Nat. Commun.* **12**, 879 (2021).
44. Hu, F. et al. Carbapenem-resistant *Klebsiella pneumoniae* capsular types, antibiotic resistance and virulence factors in China: a longitudinal, multi-centre study. *Nat. Microbiol.* **9**, 814–829 (2024).
45. Yang, X. et al. Molecular epidemiology of carbapenem-resistant hypervirulent *Klebsiella pneumoniae* in China. *Emerg. Microbes Infect.* **11**, 841–849 (2022).
46. Wu, K. et al. RNA interactome of hypervirulent *Klebsiella pneumoniae* reveals a small RNA inhibitor of capsular mucoviscosity and virulence. *Nat. Commun.* **15**, 6946 (2024).
47. Zhu, J., Wang, G. & Li, M. Outbreak of NDM-5-producing *Klebsiella pneumoniae* ST307: an emerging high-risk antimicrobial resistance clone in Shanghai, China. *mSystems* **9**, e0136923 (2024).
48. Xie, J. et al. Tree Visualization By One Table (tvBOT): a web application for visualizing, modifying and annotating phylogenetic trees. *Nucleic Acids Res.* **51**, W587–W592 (2023).
49. He, J. et al. Opposite evolution of pathogenicity driven by in vivo *wzc* and *wcaJ* mutations in ST11-KL64 carbapenem-resistant *Klebsiella pneumoniae*. *Drug Resist. Updat.* **66**, 100891 (2023).
50. Wang, R. et al. Increase in antioxidant capacity associated with the successful subclone of hypervirulent carbapenem-resistant *Klebsiella pneumoniae* ST11-KL64. *Nat. Commun.* **15**, 67 (2024).
51. Choi, M. J. & Ko, K. S. Loss of hypermucoviscosity and increased fitness cost in colistin-resistant *Klebsiella pneumoniae* sequence type 23 strains. *Antimicrob. Agents Chemother.* **59**, 6763–6773 (2015).
52. Lenz, A. M., Fairweather, M., Peyton, J. C., Gardner, S. A. & Cheadle, W. G. Liver injury and abscess formation in secondary murine peritonitis. *Inflamm. Res.* **60**, 337–345 (2011).
53. Ren, Y. et al. Majorbio cloud: a one-stop, comprehensive bioinformatic platform for multiomics analyses. *Imeta* **1**, e12 (2022).
54. Langmead, B. & Salzberg, S. L. Fast gapped-read alignment with Bowtie 2. *Nat. Methods* **9**, 357–359 (2012).
55. Li, B. & Dewey, C. N. RSEM: accurate transcript quantification from RNA-Seq data with or without a reference genome. *BMC Bioinf.* **12**, 323 (2011).
56. Love, M. I., Huber, W. & Anders, S. Moderated estimation of fold change and dispersion for RNA-seq data with DESeq2. *Genome Biol.* **15**, 550 (2014).
57. Klopfenstein, D. V. et al. GOATOOLS: a Python library for gene ontology analyses. *Sci. Rep.* **8**, 10872 (2018).
58. Xie, C. et al. KOBAS 2.0: a web server for annotation and identification of enriched pathways and diseases. *Nucleic Acids Res.* **39**, W316–W322 (2011).
59. Li, T. et al. Adaptive evolution of extensive drug resistance and persistence in epidemic ST11 KPC-producing *Klebsiella pneumoniae* during antimicrobial chemotherapy. *Antimicrob. Agents Chemother.* **10**, e0123524 (2024).
60. Zeng, J. et al. A broadly applicable, stress-mediated bacterial death pathway regulated by the phosphotransferase system (PTS) and the cAMP-Crp cascade. *Proc. Natl. Acad. Sci. USA* **119**, e2118566119 (2022).

Acknowledgements

This work was supported by the National Key Research and Development Program (No. 2023YFC2306200 to M.L.) and the National Natural Science Foundation of China (81702062 to J.Z., W2411070 and 82172325 to M.L.).

Author contributions

M.L. and J.Z. conceived and designed the experiments. J.Z. and G.W. conducted the experiments. W.X., Z.S., Q.W. and Q.F. collected the isolates. J.Z. and G.W. carried out the animal experiment. J.Z. analyzed the data and drafted the manuscript. M.L. revised the manuscript. M.L. provided grant support. All authors read and approved the final manuscript.

Competing interests

The authors declare no competing interests.

Additional information

Supplementary information The online version contains supplementary material available at <https://doi.org/10.1038/s41467-025-61379-9>.

Correspondence and requests for materials should be addressed to Min Li.

Peer review information *Nature Communications* thanks the anonymous reviewers for their contribution to the peer review of this work. A peer review file is available.

Reprints and permissions information is available at <http://www.nature.com/reprints>

Publisher's note Springer Nature remains neutral with regard to jurisdictional claims in published maps and institutional affiliations.

Open Access This article is licensed under a Creative Commons Attribution-NonCommercial-NoDerivatives 4.0 International License, which permits any non-commercial use, sharing, distribution and reproduction in any medium or format, as long as you give appropriate credit to the original author(s) and the source, provide a link to the Creative Commons licence, and indicate if you modified the licensed material. You do not have permission under this licence to share adapted material derived from this article or parts of it. The images or other third party material in this article are included in the article's Creative Commons licence, unless indicated otherwise in a credit line to the material. If material is not included in the article's Creative Commons licence and your intended use is not permitted by statutory regulation or exceeds the permitted use, you will need to obtain permission directly from the copyright holder. To view a copy of this licence, visit <http://creativecommons.org/licenses/by-nc-nd/4.0/>.

© The Author(s) 2025